

STABILIZING A LAMINAR BOUNDARY-LAYER USING PLASMA-ACTUATORS

S. Grundmann, S. Klumpp, C. Tropea
Institute of Fluidmechanics and Aerodynamics,
Technische Universität Darmstadt

Keywords: *plasma-actuator, boundary-layer, transition, stabilizing*

Abstract

This is a fundamental study about the influence of plasma-actuators on boundary-layer flows, including both experimental and numerical investigations. The actuator is placed in a boundary-layer of a flat plate and imparts momentum to the flow, resulting in a deformation of the velocity profile. The curvature of the velocity profile is amplified which leads to a more stable boundary layer with a higher critical Reynolds number. The effect of the altered velocity profile decays downstream since the actuator imparts momentum only at a given position. However, the influence on the velocity profile remains long enough to damp the growth of disturbances and to delay transition over a considerable length.

1 The Plasma actuator

Plasma actuators consist of two electrodes separated by insulation covering the lower electrode completely, while the upper one remains exposed to the flow. They are driven by a high frequency AC-voltage of several thousand volts and several thousand Hertz. The actuator generates a body force tangential to the surface which provides a variety of possibilities to manipulate or to create flows. In quiescent fluid, this force creates a wall jet with a velocity of several meters per second. With a mean flow, the actuator can be used to impart momentum into boundary layers and to alter their velocity profile, their turbulence distribution or to promote transition from a laminar to turbulent. The amplitude of the force can be altered by varying the driving voltage.

1.1 The physical working principle

The physical working principle has been described by Font [3]. During the first half-cycle, the upper electrode is negative and the high voltage causes it to emit electrons which ionize the neutral air molecules on their way to the lower electrode of opposite charge. A weakly ionized plasma is generated. The electrons gather on the insulation film of the lower electrode, while the predominantly positive ions are accelerated towards the negative upper electrode. Colliding with neutral air molecules, they transfer their momentum to the air and cause a body force affecting the air. This body force is directed opposite to the observed wall jet. These electrons gather on the insulation film, like on a barrier and build up a secondary potential, which limits the intensity of the electric field. This feature gives the plasma its name: Dielectric Barrier Discharge Plasma.

After the change of the polarity of the driving voltage, the number of electrons is one order higher than that present at the beginning of the first half-cycle. Therefore the number of ions created by the moving electrons is much higher during the second half-cycle than that during the first. The ions now move towards the lower electrode: due to their larger number they cause a body force about ten times larger than that in the first half-cycle. This time the force is in the same direction as the observed flow. The electrons can reach the upper exposed electrode and are neutralized. That is the reason why the next cycle starts again with a small number of

electrons. After one entire cycle a net force remains, causing a wall jet.

1.2 Applications of plasma-actuators

The actuators can be implemented as a single actuator or as an array of actuators. The actuators in an array can be driven with voltages of the same phase or with a phase shift between them, which causes an electrostatic wave to move along the surface. This technique results in higher wall-jet velocities than with actuators in phase [7]. Several experiments show the successful application of plasma actuators as transition strips [10], as active separation control due to transition of the flow above the suction side of airfoils [1, 4], and as wake control of bluff bodies like cylinders [8].

1.3 Current investigations

The investigations conducted at the Institute of Fluid Mechanics and Aerodynamics of the Technische Universität Darmstadt concentrate on the fundamentals of the ability of the plasma actuator to influence a flow. The goal is to determine the possibilities of manipulating boundary layers, for example promoting transition, sustaining laminar conditions or possibly even re-laminarization of a turbulent boundary layer through strong stream-wise acceleration. To achieve this, an open circuit wind tunnel has been equipped with a test section that allows measurements on a flat plate with and without a pressure gradient. Single actuators and actuator-arrays can be placed at different positions on the plate.

In this paper we present the results of our preliminary experimental and numerical investigations on the influence of plasma-actuators in the boundary-layer of a flat plate.

2 The numerical model and its calibration

To reduce the number of experiments, to design the experimental setup and to provide additional insight into the functioning of the actuators, numerical simulations accompany the experiments. To reproduce the effect of a

plasma-actuator numerically the induced body force must be modelled.

2.1 Emulating the body force

To model the actuator's body force, Jayaraman *et al.* [5] assume that the plasma only exists in a triangular region above the actuator, while no charges exist outside this region. The exact spatial charge density, the electric field strength and temporal dependency have not yet been explored, therefore several assumptions have to be made.

The governing equations are the equation for the force acting on the charges (1) and the Poisson equation (2). The charge distribution inside the triangular domain is determined by using equation (2).

$$\vec{f} = \vec{E} \rho_c e_c \quad (1)$$

$$\vec{\nabla} \cdot \vec{E} = \frac{\rho_c e_c}{\epsilon_0} \quad (2)$$

Jayaraman *et al.* [5] assume a linear decrease of the field strength with its maximum at the point of the shortest distance between the electrodes. It can be expressed by

$$|E| = E_0 - k_1 x - k_2 y \quad (3)$$

Additionally a linear growth of the triangular domain with increasing voltage is assumed. This leads to an expression for the total force acting on the flow field, which becomes negative at higher voltages. This is not reasonable and results from the fact that the linear decreasing electric field strength becomes negative at a certain distance from its maximum. To avoid this unphysical behaviour, a new distribution of the electric field has been introduced, in which the field strength approaches zero and does not become negative. The following equation is used.

$$|E| = E_0 e^{-m_1 x} e^{-m_2 y} \quad (4)$$

The gradients of the electric field should be of the same value like in the model of Jayaraman *et al.* [5]. This leads to the expressions

$$m_1 = \frac{a_0}{a_0 + b_0} \frac{\rho_{c0} e_c d}{\epsilon_0 V_0} \quad \text{and} \quad m_2 = \frac{b_0}{a_0 + b_0} \frac{\rho_{c0} e_c d}{\epsilon_0 V_0} \quad (5)$$

The field strength still has its maximum at the same point as the linear model (Eq. 3), but has an asymptotic approach to zero and therefore never becomes negative. This distribution leads to the following expression of the body force.

$$\vec{f} = \frac{\rho_{c0} V^2}{V_0 d} e^{-2(m_1 x + m_2 y)} \vec{n} e_c \quad (6)$$

This force occurs only inside the triangular domain of influence and is implemented in the Navier-Stokes equation.

2.2 Calibration Data

Since the numerical model contains several assumptions, it is necessary to calibrate three coefficients. To create an adequate data base for calibrating the developed model, PIV measurements of the flow induced by the plasma-actuator in otherwise quiescent flow have been performed.

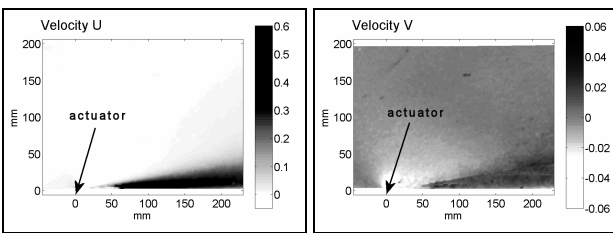


Fig. : PIV measurement of an actuator induced wall jet

Figure 1 shows the mean U and V velocities of the wall-jet created by a plasma-actuator driven by a voltage of $U_e=10\text{kVpp}$ at a frequency of $f_m=5\text{kHz}$. The left diagram of the figure 1 clearly shows the wall-jet that grows in thickness with increasing x -coordinate. In the range $0 < x < 50\text{mm}$ the wall-jet and the entrained air are apparently thinner than 2.1mm . In the right diagram the mean V velocity has been plotted. A distinct region of flow directed downwards at $x=0\text{mm}$ is apparent. This

demonstrates the sink-like effect of the actuator on the flow. It draws the surrounding air to the right edge of the upper electrode and diverts it away tangential to the wall. Downstream the jet diverges due to deceleration and mixes with the surrounding air, yielding positive V velocities.

2.3 Calibration of the numerical Model

The numerical simulations have been carried out on a 2D grid of 5500 cells with the SST-turbulence model and the low Reynolds treatment that the solver *Fluent* provides for boundary layers. The inlet boundary conditions were set to laminar with a turbulent viscosity ratio of one.

The product of the momentum flow rate and the mass flow rate is constant for a wall-jet. Therefore it is justified to calibrate the model at a single downstream position of the jet. To adjust the charge density ρ_c , within the triangular region of influence of height $a_0(V=V_0)$ and length $b_0(V=V_0)$, the maximum horizontal velocities at $x=100\text{mm}$ were examined and the model coefficients were tuned until the simulations showed the same magnitude for all measured voltages. All following simulations were conducted with these coefficients.

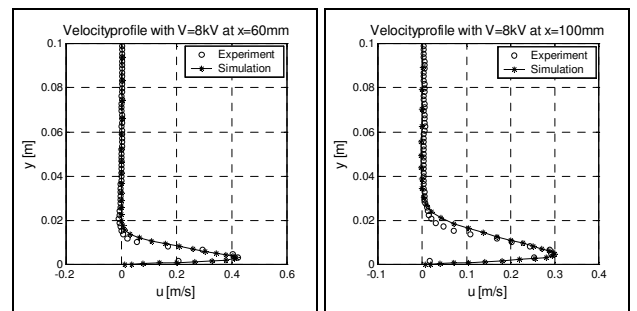


Fig. 2: Comparison of the velocity profiles

The entrainment of surrounding air by the wall jet is highly sensitive to changes of the viscosity of the fluid. Especially at low velocities, like in these experiments, the choice of turbulence model and wall treatment also has a strong influence on the numerical viscosity of the fluid. Figure 2 shows the velocity profiles at the downstream positions $x=60\text{mm}$ and

$x=100\text{mm}$, showing rather good agreement between experiment and simulations.

In figure 3 the measured and simulated momentum flux is shown as a function of downstream distance. The y-resolution of the PIV measurements ($y_{min}=2.1\text{mm}$) is too coarse to resolve the wall-jet completely below $x=100\text{mm}$, and this is responsible for the larger variations between experiment and simulations in this region. The sudden rise of the momentum transport at $x=0$ could also not be measured for the same reason.

Downstream of $x=100$ the experimental and numerical results in figure 3 agree well enough to conclude that the model is adequately calibrated to proceed with the simulations of the subsequent experiments.

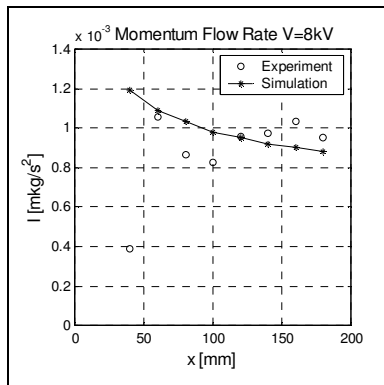


Fig. 3: Momentum flux

3 Stability of Boundary-Layers

In this section some summary remarks will be made about the stability of boundary layers in general, as a framework within which the experimental and numerical results obtained using plasma actuators can be evaluated.

The overall frictional force on a surface is given by integrating the wall shear stress

$$\tau_w = \eta \left. \frac{\partial u}{\partial y} \right|_{y=0} \quad (7)$$

over the wetted area. Obviously, the velocity gradient at the wall is the determining factor in this equation and therefore it is interesting to relate the influence of the plasma actuators on this gradient, either directly or indirectly.

It is well understood that a laminar boundary layer (Blasius profile) exhibits for the same free-stream velocity a significantly lower wall shear stress than a turbulent boundary layer; hence preventing or delaying transition from the laminar to the turbulent state will also have a direct affect on the overall wall friction.

Transition is related to the critical Reynolds number, $Re_{\delta_1, \text{krit}}$ being based on the displacement thickness of the boundary-layer profile, defined by:

$$\delta_1 = \int_0^{\delta} \left(1 - \frac{u}{U_\infty}\right) dy \quad (8)$$

Below this critical Reynolds number disturbances are damped, while above, they are amplified.

The displacement thickness δ_1 grows with downstream distance, measured from the beginning of the boundary layer where $\delta_1=0$. The local Reynolds number increases proportional to this growth until the critical Reynolds number is reached and the transition begins.

This mechanism shows the first possibility to delay the point of transition: Reducing or stopping the growth of the laminar boundary layer prevents the local Reynolds number from reaching the critical Reynolds number. This can be achieved by suction or blowing. Any other form of imparting momentum into the near-wall layer is also an alternative, as demonstrated by Weier [11] using electromagnetic forces in weakly conducting fluids. Plasma actuators used in air can be directly compared to magneto-fluid-dynamic (MFD) actuators. The major difference is that the MFD actuators can be implemented to create a continuous force along arbitrary lengths while the plasma actuators used in this work impart a body force locally at a discrete position. Therefore the growth of the boundary-layer thickness can not be completely suppressed, but the thickness can be abruptly reduced followed by a resumption of the growth.

Another strategy to delay transition is to increase the critical Reynolds number of the

local velocity profile. The critical Reynolds number can be determined approximately by using linear stability theory for boundary layers. One result of the stability analysis is that profiles with a convex curvature will damp disturbances more efficiently than more linear profiles (Reed et al. [6]). The linear stability theory is based on the boundary layer equations of Prandtl. The equation in x -direction at the wall with $y=0$ can be written as:

$$\eta \frac{\partial^2 u}{\partial y^2} = \rho v_w \frac{\partial u}{\partial y} + \frac{dp}{dx} - \frac{d\eta}{dT} \frac{\partial T}{\partial y} \frac{\partial u}{\partial y} - F \quad (9)$$

A convex curvature corresponds to a negative second derivative of the wall parallel velocity. Equation 9 shows the different options to increase the curvature. Suction through a porous wall creates a negative wall-normal velocity v_w , a negative pressure gradient is also effective as stabilizing factor, and a positive wall-normal temperature gradient together with a positive temperature dependency of the viscosity increases the curvature as well. A body force F can increase the curvature, which is the mechanism by which the plasma actuator can stabilize a boundary layer.

The critical Reynolds number of the velocity profile influenced by any of the above-mentioned factors can be determined through a stability analysis using the Orr-Sommerfeld-equation. While this procedure is usually rather complex, another possibility is to determine the critical Reynolds number empirically. Figure 4 shows the experimentally determined critical Reynolds numbers for velocity profiles of different flows depending on the shape factor H_{12} (Stuart [9], Drazin and Reid [2], White [12] and Weier [11], where the shape factor is given by:

$$H_{12} = \frac{\delta_1}{\delta_2} = \frac{\int_0^\delta (1 - \frac{u}{U_\infty}) dy}{\int_0^\delta \frac{u}{U_\infty} (1 - \frac{u}{U_\infty}) dy} \quad (10)$$

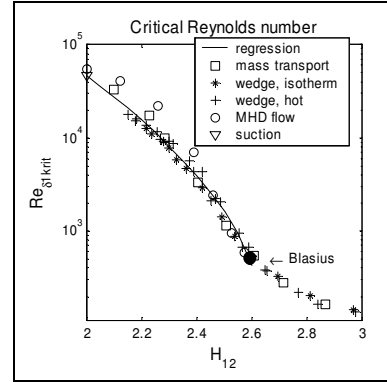


Fig. 4: Critical Reynolds number

The excellent correlation between critical Reynolds number and shape factor leads to the conclusion that the shape factor can be considered a good indicator of stability. The Blasius profile has a shape factor of $H_{12}=2.59$, lower shape factors indicate a profile with a stronger negative curvature.

Another family of self-similar velocity profiles is given by the Falkner-Skan-solution to the flow over a two-dimensional wedge.

$$f''' + f f'' + \beta_H (1 - f'^2) = 0 \quad (11)$$

where β_H is the opening half-angle of the wedge.

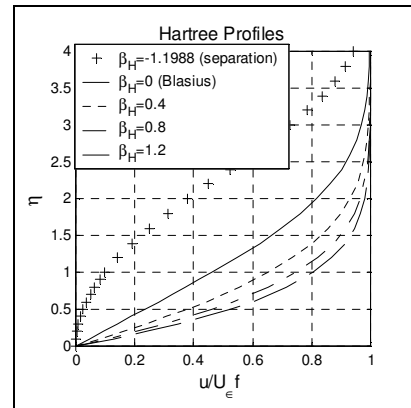


Fig. 5: Falkner-Skan velocity profiles

The Blasius-equation for a boundary layer over a flat plate with zero pressure gradient is obtained when $\beta_H=0$. The additional term in the Falkner-Skan-solution relates to a non-zero pressure gradient existing for wedge flows, hence β_H can be considered also a pressure gradient parameter. Negative values of β_H represent an adverse pressure gradient.

A boundary layer with $\beta_H = -0.1988$ has a velocity profile intersecting the wall at right angles and is therefore a separation point. Figure 5 illustrates solutions to the Falkner-Skan equations as a function of β_H . Profiles with positive β_H values correspond to an accelerated boundary layer (favourable pressure gradient) and exhibit a higher critical Reynolds number, as can be seen in figure 4.

4 Experimental and Numerical Investigations

4.1 Experimental Investigations

The following experiments have been conducted on a flat plate with zero pressure gradient. The wind tunnel has a test section of 0.45m width and 0.45m height. The plate is placed in the middle of the test section and the leading edge has an elliptic profile to prevent the flow from separating. The plasma-actuator is placed 150mm downstream of the leading edge, oriented in the spanwise direction. To maintain a smooth surface the actuator is fitted into a notch in the plate.

The velocity profiles are measured at the positions 40mm, 60mm and 80mm downstream of the actuator. The measurements were performed with two constant temperature hot-wire probes (CTA). Both signals are linearised by an analog amplifier and are passed through a low-pass filter to avoid aliasing effects when digitized. Both probes are mounted on a single traversing system with a vertical separation of 40mm. The lower probe is traversed throughout the boundary layer, while the upper one measures the free-stream velocity, which is necessary to compensate for velocity fluctuations due to weather influences on the wind tunnel at low speeds (the tunnel draws air directly from outside the laboratory).

The electric field of the actuator disturbs the CTA measurements leading to an apparent turbulence, while the mean value is not influenced. The magnitude of this offset of the measured variance of the velocity fluctuations is independent of the local velocity; hence it is treated as system noise and it can be removed in the signal processing step.

4.1.1 Quantifying the actuator effect

Experiments have been carried out for a free-stream velocity between 6m/s and 12m/s, for which the boundary layer is laminar at the actuator position. The resulting Reynolds number based on the displacement thickness at the position of the actuator varies between 350 and 700.

The actuator adds momentum to the boundary layer which leads to a deformation of the velocity profile, as exemplarily illustrated in figure 6. The momentum flux difference caused by the plasma actuator can be computed by integrating the difference of the velocity profiles. This momentum flux difference is shown in figure 7 as a function of free-stream velocity and downstream position.

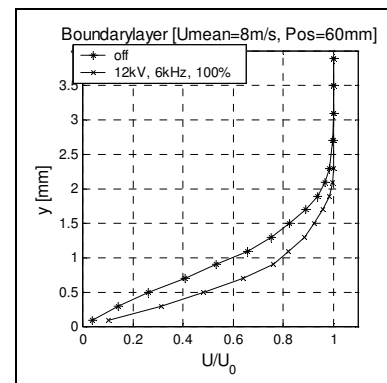


Fig. 6: Boundary layer with and without plasma actuator activated

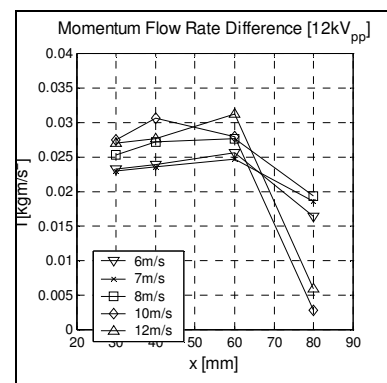


Fig. 7: Momentum flux differences

The difference in momentum flux close to the actuator is approximately independent of free-stream velocity. The relative influence of this added momentum can be better appreciated by relating the added momentum to the

momentum deficit of the unaffected boundary layer at that downstream position, expressed by the momentum thickness. This is very similar to the non-dimensional Hartmann number, Z , used for magneto-fluid-dynamical flows. The Hartmann number relates the electromagnetic force of a MFD actuator to the wall friction force of the affected boundary layer. At a Hartmann number of one the momentum loss due to wall friction is exactly compensated by the imparted force by the magnetic field and the growth of the boundary layer is stopped. Since the plasma actuator does not create a continuous force but a local acceleration it is necessary to modify the Hartmann number for the use with plasma actuators. We define the modified Hartmann Number as follows:

$$Z_m = \frac{\Delta \dot{I}}{\frac{1}{2} \rho U_\infty^2 \cdot \delta_2}, \quad (12)$$

where $\Delta \dot{I}$ is the difference in the momentum flux caused by the actuator.

A modified Hartmann number of one corresponds to the situation when the actuator adds as much momentum to the boundary layer as it would have lost at the downstream position of the actuator without the actuator turned on.

4.1.2 The stabilizing effect

Figure 8 shows the development of the measured boundary layer velocity profiles at the positions $x=40\text{mm}$, $x=60\text{mm}$ and $x=80\text{mm}$. A modified Hartmann number of $Z_m=1.45$ has been used. The profiles are plotted for the flow with the actuator turned on and off. Additionally the Blasius profile has been overlaid to confirm that the boundary layer without actuator is indeed a zero-pressure gradient boundary layer. For each position, one solution of the Falkner-Skan equation has been included, selecting β_H to best match the experimental profile.

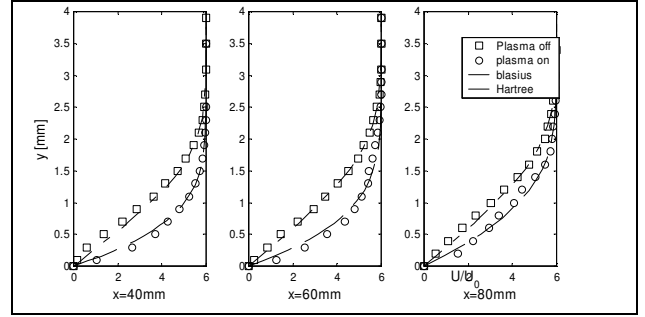


Fig. 8 Measured and theoretical velocity profiles

The good agreement of the velocity profile with the actuator turned on with the Falkner-Skan profile demonstrates that the stabilizing effect of the plasma actuator is equivalent to the stabilizing effect of a negative pressure gradient. The following table summarizes the corresponding wedge angles, the shape parameter H_{12} and the critical Reynolds numbers (from figure 4) for the three profiles.

Pos [mm]	β_H	H_{12}	$Re_{\delta_1 \text{ crit.}}$
40	0.80	2.08	30751
60	0.75	1.93	63942
80	0.35	2.20	15511
Blasius	0.00	2.59	520

The development of the shape factor and the critical Reynolds number shows that the velocity profile is changed by the actuator to a more stable profile. Since the actuator creates the volume force over a very short length the effect decays as the flow moves on. But the affected boundary layer can damp existing disturbances over a considerable distance before it returns asymptotically to the less stable Blasius profile.

4.2 Numerical Investigations

The numerical investigation of the experimental setup was conducted on a 2D-grid of 156000 cells. The turbulence intensity of the inlet data was set to $T_i=0.3\%$, which is the turbulence intensity of the wind tunnel. An SST turbulence model with the Low-Reynolds treatment in the commercial code *Fluent* was used. The grid is a simple rectangle with a no-slip wall on the lower boundary, a constant velocity inlet at the left side, a symmetry plane

on the upper side and a constant pressure outlet on the right side.

Figure 9 shows the development of the measured and simulated boundary layer at the positions $x=40\text{mm}$, $x=60\text{mm}$ and $x=80\text{mm}$. The profiles are plotted for the flow with the actuator turned on and off.

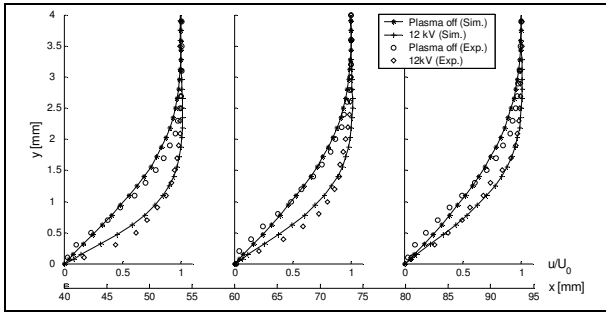


Fig. 9 Measured and simulated velocity profiles

The comparison of the measured and simulated profiles shows very good agreement. The simulations described in the following were performed for a configuration with the position of the plasma actuator 300mm downstream of the leading edge.

4.2.1 Maximum delay of transition

To determine the highest attainable delay of transition, a numerical parametric study has been performed. The driving voltage of the actuator has been varied for a constant free-stream velocity of 6m/s. To determine the point of transition the plot of friction coefficient or boundary thickness can be used. Figure 10 shows an example of these diagrams.

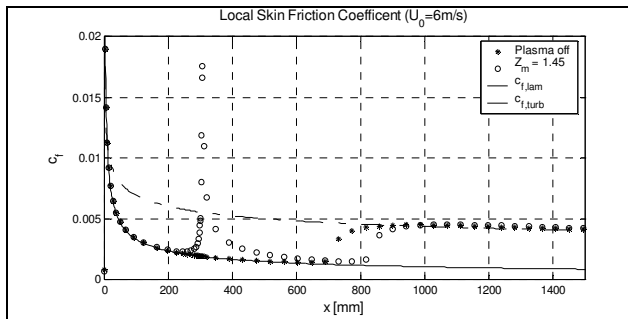


Fig. 10: Wall friction coefficient with and without plasma actuator

This diagram shows the shift of the point of transition from $x=705\text{mm}$ to $x=830\text{mm}$. The unaffected flow follows exactly the theoretical

course of a laminar boundary layer up until $x=705\text{mm}$. When the plasma actuator is activated, the local skin friction initially increases directly downstream, caused by the higher near-wall velocities. The skin-friction then relaxes to the undisturbed laminar value before undergoing transition. The net benefit of transition delay in terms of reduced friction is partially reduced by the increased friction downstream of the actuator.

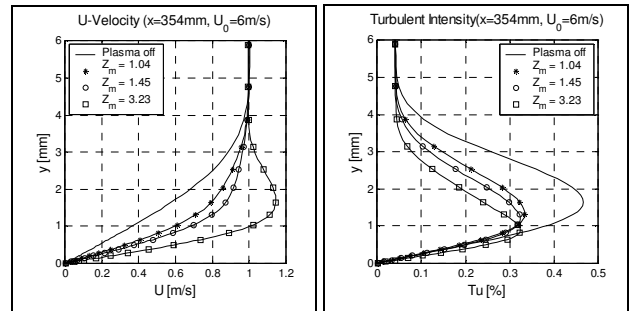


Fig. 11: a) Velocity and b) k-profiles 54mm downstream of the actuator

A comparison of different strong accelerations by the actuator is given in figure 11 for the velocity profiles and the turbulence intensity. Figure 11b demonstrates the damping effect on the turbulent fluctuations through the acceleration when the actuator is turned on. The maximum delay of the point of transition does not occur at the highest driving voltage as figure 11a indicates. The reason for this is the velocity overshoot that appears for very strong accelerations (Hartmann numbers).

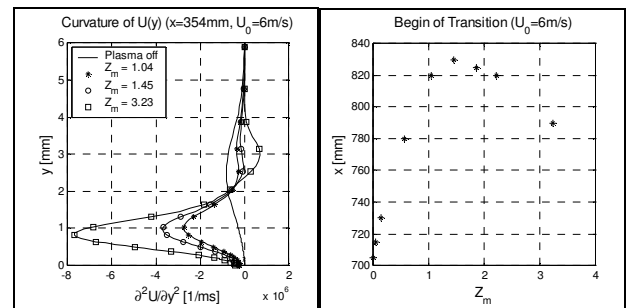


Fig.12: Curvature of velocity profiles Fig.13: Position of transition

Figure 12 shows the curvature of the velocity profile for different Hartmann numbers. A negative curvature is known to be stabilizing, while velocity profiles with inflection points are

unstable and lead quickly to transition. Only the curvature of the profile with overshoot shows an inflection point together with a positive curvature. This leads to an unstable region of the velocity profile where disturbances can be amplified. The conclusion is that the actuator works most efficient for transition delay with the highest driving voltage that does not lead to an overshoot in the velocity profile. This corresponds to a Hartmann number of $Z_m=1.45$. That means the actuator imparts 45% more momentum to the boundary layer than it has lost due to friction at the wall.

Since the actuator does add momentum at a single position the effect on the boundary layer decays downstream of the actuator. One way to determine the length, on which the stabilizing influence of the actuator is still present, is to plot the development of the shape factor H_{12} of the boundary-layer profile.

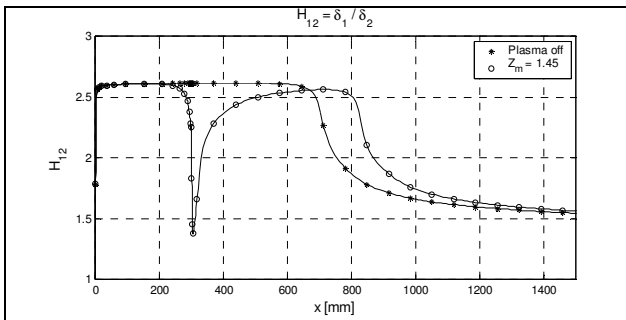


Fig. 14: Shape factor of the boundary-layer with and without the plasma actuator activated

The value of H_{12} can be understood as a criterion for the ability of a boundary-layer to damp disturbances. Figure 14 shows this plot with the actuator turned on and off. Another possibility to clarify the influence on the boundary layer is the diagram in figure 15. As discussed above, the critical Reynolds number of each profile can be determined through the shape factor with the help of the diagram shown in figure 4. Using the shape factor of figure 14, the critical Reynolds number of the flows with and without the actuator has been determined and plotted in figure 15. Additionally, the local Reynolds numbers based on the displacement thickness δ_1 has been plotted. The comparison of the development of the local Reynolds number with the critical Reynolds number

shows that Re_{δ_1} exceeds $Re_{\delta_1 \text{ krit}}$ already upstream of the actuator. It remains above the critical Reynolds number and indicates that the amplification of disturbances will begin. With the actuator turned on, $Re_{\delta_1 \text{ krit}}$ increases rapidly while Re_{δ_1} decreases.

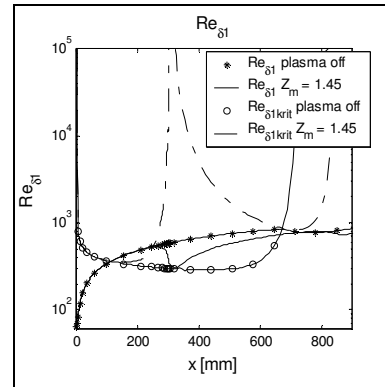


Fig.15 Reynolds number and critical Reynolds number

The local Reynolds number is only higher than the critical value over a short distance. The actuator can clearly delay reaching of the critical Reynolds number. A diagram like figure 15 can be used to determine the best position for a plasma actuator or of several actuators in succession to delay transition.

Conclusions

Plasma actuators have been placed in a boundary layer of a flat plate to delay transition. The modified Hartmann number has been introduced to quantify the impact of an actuator on a boundary layer independent of the driving voltage and the free-stream velocity. The modified Hartmann number relates the momentum flux added to the boundary layer by the actuator to the momentum loss of the unaffected boundary layer.

The ability to modify the boundary layer velocity profile to a more stable condition has been demonstrated. The velocity profiles downstream of the actuator match the accelerated velocity profiles of wedge flows. The spatial extent of the stabilizing effect has been determined using the shape factor of the affected boundary layer.

The turbulence intensity of the boundary layer is damped for all Hartmann numbers.

However increasing the Hartmann number too much leads to an overshoot in the velocity profile and to an inflection point; hence to a less stable velocity profile. This effect moves the point of transition upstream.

References

- [1] Corke, T.C., He, C. (2004) Plasma Flaps and Plasma Slats: An Application of Weakly-Ionized Plasma Actuators. 2nd AIAA Flow Control Conference, Portland, Oregon, June 28-1, 2004, AIAA-2004-2127
- [2] Drazin, P.G. und Reid, W.H. (1981) Hydrodynamic Stability. Cambridge University Press, Cambridge
- [3] Font, G.I., Morgan, W. (2005) Plasma Discharges in Atmospheric Pressure Oxygen for Boundary Layer Separation Control, 35th AIAA Fluid Dynamics Conference and Exhibit, Toronto, Ontario, June 6-9, 2005, AIAA-2005-4632
- [4] Grundmann, S., Tropea, C. (2005) Gepulste Plasma Actuatoren zur aktiven Grenzschichtbeeinflussung. 12. STAB Workshop 2005, DLR Göttingen
- [5] Jayaraman, B., Shyy, W. (2003) Flow Control and Thermal Management Using Dielectric Glow Discharge Concepts. 33rd AIAA Fluid Dynamics Conference and Exhibit, Orlando, Florida, June 23-26, 2003, AIAA-2003-3712
- [6] Reed, H.L., Saric, W.S. und Arnal, D. (1996) Linear stability theory applied to boundary layers. Annu. Rev. Fluid Mech., **28**: 389_428
- [7] Roth, J.R. (2003) Aerodynamic Flow Acceleration using Paraelectric and Peristaltic Electrohydrodynamic (EHD) Effects of a One Atmosphere Uniform Glow Discharge Plasma, Physics of Plasmas, Vol. 10, No. 5
- [8] Touchard, G., Artana, G., Sosa, R., Moreau, E. (2003) Control of the near-wake flow around a circular cylinder with electrohydrodynamic actuators. Experiments in Fluids **35**:580-588
- [9] Stuart, J.T. (1963) Laminar Boundary Layers, Dover, Kap. Hydrodynamic Stability
- [10] Velkoff, H.R., Ketcham, J. (1968) Effect of an Electrostatic Field on Boundary-Layer Transition. AIAA Journal **6** (7):1381-1383.
- [11] Weier, T., (2005) Electromagnetic Flow Control using wall-parallel Lorentz-Forces in weakly conducting fluids, Ph.D. Thesis, Technische Universität Dresden
- [12] White, F.M. (1991) Viscous Fluid Flow. McGraw Hill, New York, 2. Auflage